Preprocessing-Based Fast Design of Multiple EM Structures With One Deep Neural Network

Peng Wang, *Graduate Student Member, IEEE*, Zhenning Li, Chao Luo, Zhaohui Wei, *Graduate Student Member, IEEE*, Tong Wu, Wen Jiang, *Senior Member, IEEE*, Tao Hong, *Senior Member, IEEE*, Naser Ojaroudi Parchin, *Senior Member, IEEE*, Gert Frølund Pedersen, *Senior Member, IEEE*, and Ming Shen, *Senior Member, IEEE*

***Abstract*— Deep learning (DL) plays a vital role in the design of electromagnetic (EM) structures. However, in current research, a single neural network typically supports only one structure design and requires a complex framework to accommodate multiple structure designs. This article proposes using one neural-assisted design for facilitating multiple EM structures. We use two filling methods to control the vector length, an identification method to ensure accurate prediction results, and a random auxiliary vectors method to increase the data volume and reduce loss. Subsequently, we design a forward neural network (FNN) and an inverse neural network (INN) using the proposed method. The developed neural network is used to complete the dual-passband frequency-selective surface (DP-FSS), space–time-coding digital metasurface element (STCDME), single-/dual-band absorbing metasurface (SDAM), and dual-stopband frequency-selective surface (DS-FSS) designs. The mean absolute error (MAE) loss values for FNN/INN predictions and actual results for these four structures are 0.019/0.116, 0.035/0.602, 5.14/0.146, and 0.018/0.07, respectively. Finally, we design four structures with the well-training network, fabricate DP-FSS and DS-FSS, and measure them in an anechoic chamber. The measurement and simulation results are in good agreement. The proposed method significantly reduces the complexity of multiple EM structure designs, decreases the need for multiple neural networks, and simplifies the design framework, thereby contributing to the development of AI-assisted EM structures.**

***Index Terms*— 0-vector filling, DNN, identification method, interpolation filling, multiple electromagnetic (EM), random auxiliary vector method.**

I. Introduction

TRADITIONAL metamaterials are theoretically infinite periodic structures in the horizontal plane. In practice, we can make sufficient units to exhibit properties close to the theory [1], [2]. Metamaterials are composed of uniform patches, apertures, and lumped elements, which achieve the modulation of electromagnetic (EM) waves in space, e.g., selective transmission and reflection of EM waves, changing the phase of transmission and reflection of EM waves, and absorption of EM energy [2], [3], [4]. Owing to their particular spatial EM wave adjustment property, metasurfaces have been widely applied in many microwave applications, including radomes [5], antenna reflectors [6], signal enhancement [7], beamforming [8], radar cross section (RCS) reduction [9], and so on. Different design forms and methods for EM structures have been proposed accordingly, e.g., frequency-selective surface (FSS) [1], frequency-selective rasorber (FSR) [10], space–time-coding digital metasurfaces (STCDMs) [11], polarization conversion metasurface (PCM) [9], and energy-selective surface (ESS) [12]. The conventional EM design methods require experienced designers with domain knowledge and use full-wave EM simulation software, e.g., CST, HFSS, and FEKO, to simulate and optimize, which is time-consuming and resource-demanding. The design's efficiency relies on the designers' expertise and available computational power.

In recent years, with the development of computer science, especially artificial intelligence (AI), machine learning (ML), and deep learning (DL), numerous articles have proposed AI-based methods to help automate EM design and optimization. AI-based EM structures' design is currently available in forward design [13], inverse design [14], generative design [15], and reinforcement learning design [16], the neural networks for these design being called forward neural network (FNN), inverse neural network (INN), generative neural network (GNN), and reinforcement learning neural network (RLNN), respectively.

The forward design is similar to our general EM structure design process, which obtains the EM structure S-parameters by neural network mapping EM geometric parameters and excitation [13], [17], [18], [19], [20], [21], [22], [23], [24]. In the forward design, FNN is the surrogate model, and iterative optimization was performed to find the optimal design, many EM structures are designed based on FNN, and of course, there are many studies on how to improve the neural network, e.g., how to obtain high-quality data and how to improve neural network accuracy. Wang et al. [13]

Manuscript received 25 July 2023; revised 19 February 2024; accepted 12 March 2024. Date of publication 29 March 2024; date of current version 7 May 2024. This work was supported by China Scholarship Council. *(Corresponding author: Ming Shen.)*

Peng Wang, Zhaohui Wei, Gert Frølund Pedersen, and Ming Shen are with the Department of Electronic Systems, Aalborg University, 9220 Aalborg, Denmark (e-mail: mish@es.aau.dk).

Zhenning Li and Chao Luo are with the Aerospace Information Research Institute, Chinese Academy of Sciences, Beijing 100094, China.

Tong Wu is with the College of Information Science and Electronic Engineering, Zhejiang University, Hangzhou 310027, China.

Wen Jiang and Tao Hong are with the National Key Laboratory of Antennas and Microwave Technology, Xidian University, Xi'an 710071, China.

Naser Ojaroudi Parchin is with the School of Computing Engineering and the Built Environment, Edinburgh Napier University, EH10 5DT Edinburgh, U.K.

Color versions of one or more figures in this article are available at https://doi.org/10.1109/TAP.2024.3381376.

Digital Object Identifier 10.1109/TAP.2024.3381376

propose the data cropping algorithm to reduce the data processing time and enhance the accuracy of the DNN, designing an absorptive frequency-selective transmission metasurface. Stankovi et al. [23] propose a general approach for antenna design and optimization based on the consensus of the results from several independently trained forward design DNNs. Zhang et al. [24] propose an ML-assisted antenna optimization method based on the random forest (RF) algorithm with data augmentation (DA). These novel preprocessing methods and algorithms make FNNs more powerful.

The inverse design is using structure S-parameters to obtain geometric parameters, and INN offers a new design idea for the design of EM structures, i.e., directly obtaining the structure dimensions through the target [14], [17], [18], [19], [20], [21], [22], [25], [26]. Zhu et al. [25] propose a Fourier subspace-based DL method (FS-BDLM) for FSS inverse design, where the dimension of the input is largely reduced using Fourier subspace to represent the most salient features of the desired S-parameter performance. Cong et al. [26] propose an FSS design method based on the combination of equivalent circuit model (ECM) and forward and inverse deep neural network (FIDNN). In [27], we proposed an ML-based framework, combining INN and FNN, for STCDMs' design. These inverse design methods allow the designer to obtain structures based on S-parameters, thus completing the EM design.

Generative design is generating similar samples to the ones in the training dataset and it achieves fast optimization [14], [15], [28], [29], [30]. Wang et al. [29] use three deep convolutional networks, a generator, a discriminator, and a predictor, and the well-trained GAN can generate similar samples to the ones in the training dataset (TDS) and achieve a fast optimization. Reinforcement learning design is to explore an unknown environment, collect data, and finish optimizing the structure [16], [31]. Wei et al. [31] proposed an RL-based automation design method for decoupling array antennas.

The research above has advanced the AI-assisted automated design of EM structures to various degrees. However, trained neural networks are used only to optimize and accelerate the design of one structure. Therefore, many researchers have proposed preprocessing methods and frameworks for multiple EM structures' automated designs. Naseri et al. [32] use the type code to choose each layer's form to design nonuniform bianisotropic metasurfaces. Shi et al. [33] propose a novel intelligent antenna synthesis system to realize smart antenna classification, and intelligent geometric parameter prediction is proposed based on the support vector machine (SVM). Zhou et al. [34] propose a fully automated inverse design by establishing a machine-friendly mapping flow based on principal component analysis and SVM. Shi et al. [33] and Zhou et al. [34] proposed frameworks that require two steps to complete the inverse or forward design of different structures. The first step is to identify the technology and structure to be chosen, which need one neural network for classification to analyze types, and the second step is to optimize using one regression neural network for a specific structure.

One neural network can only optimize one EM structure in the above articles. Multiple EM structures design needs complex frameworks and many neural networks. To address this problem, this article proposes achieving multiple structure designs and optimization through one neural network to simplify the design framework. To achieve the design of multiple structures through a single neural network, we used the type vector in the input to distinguish the different structures and S-parameters. To ensure the accuracy of the predictions, we also used the type vector as the output. Because neural networks have requirements for the dimensionality of the input and output vectors, we use 0-vector and linear interpolation methods to ensure uniformity in the dimensionality of the input and output vectors. And we use frequency vectors to help process the S-parameter vectors. In addition, we use the random auxiliary vector method [13] to cope with the insufficient amount of data. Repeating the data and adding a new column of random vectors to the input and output allows the neural network to train the existing data adequately, which realizes a better trained neural network with a smaller mean absolute error (MAE). The main contribution of this article is concluded as follows.

1) This article proposes the idea of the multiple EM neural network, i.e., using one neural network to help design multiple EM structures. And we design a multiple FNN and a multiple INN that present good performance. Different from [33], [34] using SVM for classification and multiple neural networks for various EM designs, this article uses only one neural network to achieve the complex framework work by suitable preprocessing methods.
2) This article proposes 0-vector filling and interpolation filling methods for dealing with different EM structures with different structural parameters and S-parameter dimensionality vectors. This solves the problem of designing dimensionality for one neural network with multiple structures.
3) This article proposes that the identification vector increases the reliability of the neural network. Inspired by the AE, we added structure and S-parameter identification vectors to both the input and output to ensure correct prediction of each structure size and S-parameter. This solves the problem of distinguishing different structures and parameters and ensuring accuracy for one neural network with multiple structures.
4) Wang et al. [13] propose the data cropping algorithm to increase the data number and divide data into augmented and simulated data. This article follows the approach of [13] but drops the cropping process and increases the data number by directly introducing a random vector, improving the neural network performance.

This work is organized as follows. Section II introduces concepts of DNN and forward/inverse design. Section III introduces the preprocessing method for multiple EM structures' design with only one neural network, i.e., 0-vector filling, interpolation filling, identification vector, and random auxiliary vector methods. Section IV uses example designs to validate the proposed method.

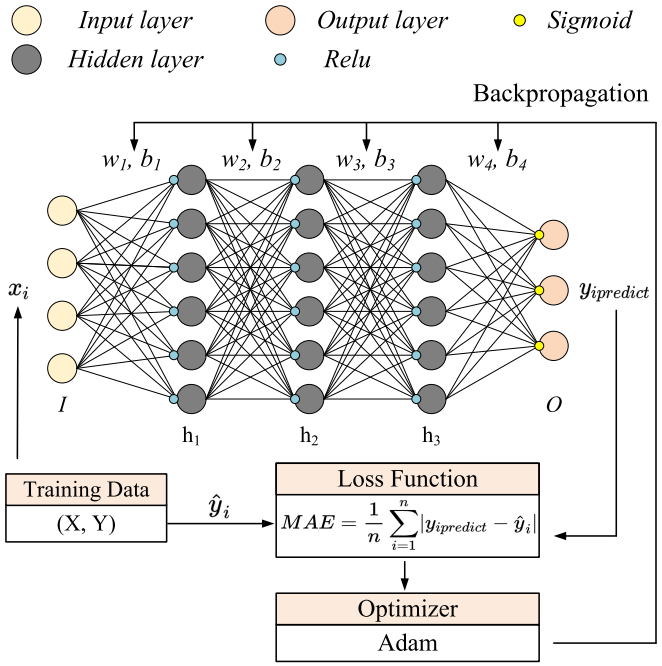

Fig. 1. DNN and its training process.

II. Deep Neural Network for EM Design

A. DNN

The perceptron is a signal transmission network consisting of sensory units, association units (hidden layer), and output or response units [35]. A feedforward fully connected DNN is essentially a perceptron containing multiple hidden layers, as shown in Fig. 1, which is a schematic representation of the structure of a DNN having three hidden layers. DNNs use a hierarchical structure, i.e., the input, hidden, and output layers. Adjacent layers are fully connected, with no connection between nodes in the same layer. The value of each node in each layer is a linear weighted sum of the previous layer's node value and the current layer weight value, which is then obtained by an activation function. For a DNN with L hidden layers, here we consider the input as layer 0, $X = h^0$, and the output as layer L + 1, $Y = h^{L+1}$, then the values of each layer are calculated as follows:

$$h^l = f(w^l * h^{l-1} + b^l), \quad 1 \le l \le L+1 \tag{1}$$

where w^l and b^l are the weights and bias vectors of the lth layer of the DNN, respectively. $f(\cdot)$ is the activation function, which we use in this article are rectified linear unit (ReLU) and sigmoid. It is calculated as (2) and (3). The activation function introduces nonlinear variation to the neural network computation, allowing the network to learn complex nonlinear relationships

$$\text{ReLU}: f(x) = \max(x, 0) \tag{2}$$

$$\text{sigmoid}: f(x) = \frac{e^x}{1+e^{-x}}. \tag{3}$$

With the weights, bias vectors, and the activation function, for an input vector x_i, we can obtain an output vector, i.e., the prediction result $y_{ipredict}$. The training process of DNN is shown in Fig. 1, where we calculate the difference value between the actual value y and the predicted result $y_{ipredict}$ by a loss function, such as MAE. This value is used as the optimization target for the algorithm, and this difference is minimized by adjusting the model parameters (e.g., weights and bias), a process known as backpropagation. The optimizer constantly updates the model's parameters, eventually making the model's prediction results close to the actual value, which is the process of DNN training.

B. Forward and Inverse Design of EM Structure

The forward design of EM structures is obtaining the structure's working performances in the given environment. We determine the EM structure form, dimensions, and operating environment for the traditional forward design process and solve the Maxwell equations to derive the S-parameters, radiation parameters, scattering cross section, etc. Generally, we use computer software to complete the calculation process.

According to Section I, with the development of computer science, DL provides new design and solution ideas for the design of EM structures. With neural networks, we can quickly obtain the S-parameters of a structure. This article proposes the method for the design of multiple EM structures through one neural network. Equations (4)–(6) show the expressions for obtaining multiple EM structure S-parameters and geometric parameters by one neural network, i.e., forward and inverse designs' expressions

$$S = f(d) \tag{4}$$

$$(t, S, r) = f(t, f, d, r) \tag{5}$$

$$(t, x, r) = f(t, f, S, r) \tag{6}$$

where t is an identification vector containing information about the structure and S-parameter type, S denotes the S-parameters of the structure, d is the geometric parameters of the structure, f is a frequency vector to assist in S-parameter dimensional changes, and r is a random vector to supplement the data to enhance network training. Equations (4) and (5) are mappings of the EM structure forward design. Equation (4) is a conventional mapping of the equations for the design of EM structures. It means one geometric parameter of the structure corresponding to its S-parameters, i.e., we get the corresponding S-parameters by assigning values to the designed structure's geometric parameter. Equations (5) and (6) are the mapping of multiple EM structures' forward and inverse designs, respectively, where we use the t vector to distinguish the different structures and S-parameters.

III. Data Preprocessing Method for Multiple EM Design With One Network

Currently, DL-assisted EM structure designs use one neural network to help design one structure, and some works use complex frameworks to achieve different EM structure designs. Here, we introduce the idea of using one neural network to help design multiple EM structures, simplifying the complex framework. The main problems for one neural network designing multiple EM structures are that different

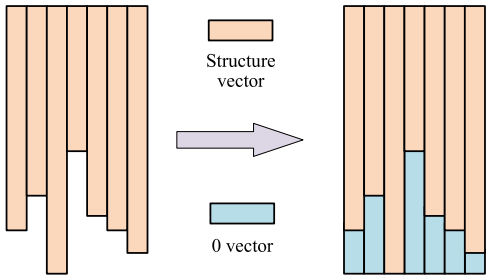

Fig. 2. 0-vector filling method.

EM structures have different dimensional vectors, and we need to distinguish different EM structure predictions, and more data for the neural network. Here, we propose the following methods, i.e., filling, identification, and random auxiliary vector methods, to solve these problems.

A. Filling Methods

Neural networks have strict requirements on the dimensionality of the input and output data, i.e., the same neural network can only process parameters of a defined dimension. Therefore, to implement a neural network for forward or inverse prediction of different structures, it is necessary to ensure that the structure geometric parameters and S-parameters are in the same dimension. However, in EM design, different structures have their own parameters and frequencies, and it is impossible to ensure that each structure has the same dimensional and frequency parameters. Hence, the dimensional unity preprocessing methods, i.e., the 0-vector filling and line interpolation methods, are proposed to address this problem.

In 0-vector padding, i.e., for structure or S-parameter vectors of different lengths, we supplement the vectors with zeros to make the vectors of the same length. Here, we use the structure geometric parameters as an example. Structure geometric parameters' dimensional unity preprocessing is to unify vector dimensions to $d_{\max}$ ($d_{\max} = \max(\dim(d_i)), 1 \leq i \leq m$), in which $d_{\max}$ is the largest size dimension number corresponding to the m structures. d_i is the ith structure original dimension vector. We combine the vector d_i with a certain length's 0-vector to obtain the processed vector d_i'. The length of the 0-vector is calculated by $d_{\max}$ and the length of d_i vector. Finally, we get the dimensional unity geometric parameters D_m'. The process of the 0-vector filling method is shown in Fig. 2.

The interpolation filling method uses linear interpolation to change the dimensionality of the existing data (e.g., S-parameter vectors). The S-parameter frequency point can be set by software, but once the requirements change, these generated data cannot be reused. Therefore, we fix the simulation step size and make the S-parameters of different structures of the same dimension by preprocessing methods. To assist design, we introduce a frequency matrix F, consisting of each structure's maximum and minimum operating frequency points. The original S-parameter vector s_i^n and the S-parameter vector s_i^p by interpolation filling method have the same start and stop frequency points. We calculate the bandwidth of the ith structure and divide the frequency bands evenly so that the number of frequency points changes from n to p

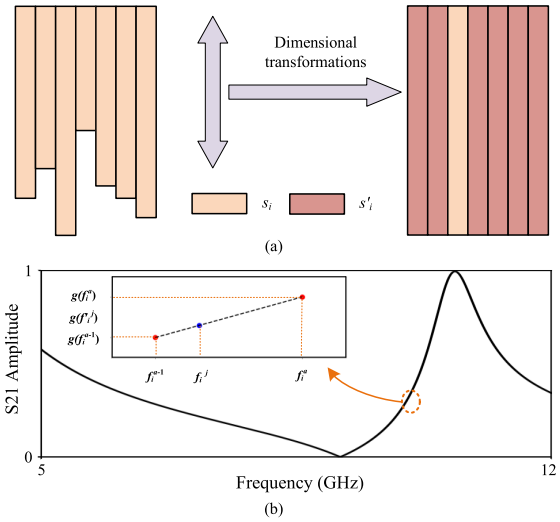

Fig. 3. Linear interpolation method for S-parameters' dimensional unity. (a) Matrix diagram. (b) Vector interpolation diagram.

$$s_i = s_i^n = \left(g\left(f_i^1\right), \ldots, g\left(f_i^j\right), \ldots, g\left(f_i^n\right)\right) \tag{7}$$

$$g(f_i'^j) = g\left(f_i^{a-1}\right) + \left[g\left(f_i^a\right) - g\left(f_i^{a-1}\right)\right]d \tag{8}$$

$$d = \left(f_i'^j - f_i^{a-1}\right) \Big/ \left(f_i^a - f_i^{a-1}\right) \tag{9}$$

$$f_i'^j \epsilon \left(f_i^{a-1}, f_i^a\right] \tag{10}$$

$$s_i' = s_i'^p = \left(g\left(f_i'^1\right), \ldots, g\left(f_i'^j\right), \ldots, g\left(f_i'^p\right)\right). \tag{11}$$

The S-parameter values for the generated frequency points are calculated by referring to (7)–(11), where f^j is the frequency corresponding to the jth frequency point, and $g(f^j)$ is the mapping relationship between the frequency and the S-parameter. p ($p = \max(\dim(s_i)), 1 \leq i \leq m$) is the maximum dimensionality of all structure S-parameter vectors, which is actually the maximum working frequency range. The process of the line interpolation method for S-parameters is shown in Fig. 3.

B. Identification Method

How to ensure accurate predictions is another concern for designing. We added identification vectors to the structure geometric parameters and S-parameters to solve this problem. The identification vectors are used to assist the neural network for multiple structures' prediction and to ensure the correctness of the prediction results.

The identification vector is inspired by the autoencoder (AE) in Fig. 4(a), whose input vector is the same as the output vector. We add the identification vector X_2 to the original inputs and outputs (X_3, Y_3) in Fig. 4(b), thus obtaining the new inputs and outputs (X, Y). The identification vector plays the role of classification and identification. The identification vector allows us to know which structure and S-parameters the predicted outcome will be. By comparing the input and output identification vectors, we confirm whether the neural network prediction results are correct and decide the next

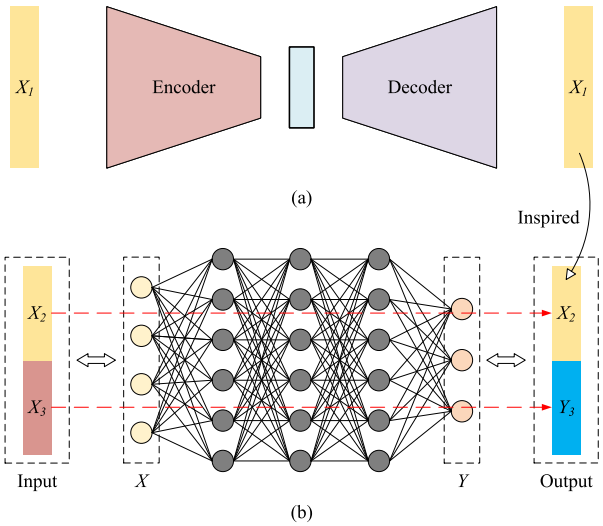

Fig. 4. (a) AE network. (b) DNN input and output data preprocessing with identification vector.

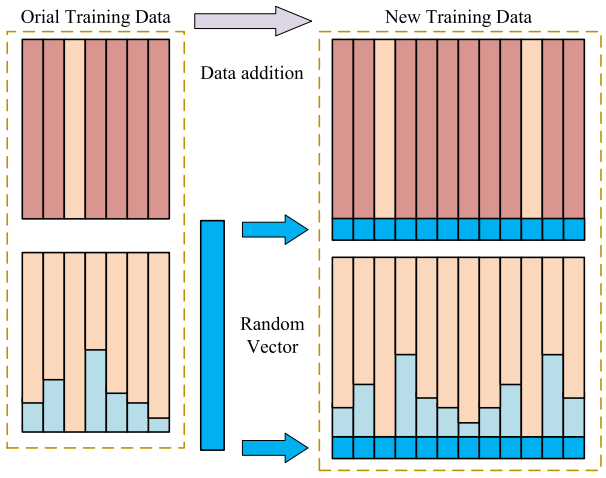

Fig. 5. Add additional random vector to increase data number.

step. In addition, Fig. 4(b) focuses not on the network but on processing the training data, i.e., input and output. Fig. 4(b) demonstrates the DNN in only the network layer portion for illustrative purposes. The detail of the DNN training process is shown in Fig. 1.

Although the form of the identification vector is the same as the AE input and output, it is worth noting and pointing out that AE is a neural network used for processing data such as data denoising. The identification vector is a preprocessing method to achieve different classes of predictions. Using the identification vector makes the classification and regression work into one neural network, avoiding the need for complex framework designs.

C. Random Auxiliary Vector Method

The training data and the quality of the training data influence how well the network model is trained. Some works have investigated how to obtain high-quality data to reduce the amount of data required by the model [13], [36]. Wang et al. [13] propose the data cropping algorithm. The simulated data are cropped and replaced with random data. Here, we do not crop the data but add an additional random vector to increase the data number. This is shown in Fig. 5. We randomly select a certain percentage of the original data and add an auxiliary random vector to the original data and the extracted data to form a new training dataset.

IV. Multiple EM Design Based on Proposed Method

A. Example 1: Multiple EM Structures Forward Designs

In this section, we use the proposed methods to complete the forward design of multiple EM structures by the proposed preprocessing method. Different EM structural models are shown in Fig. 6, where Fig. 6(a)–(d) shows the structural model of a dual-passband FSS (DP-FSS), a single-/dual-band absorbing metasurface (SDAM), an STCDM element (STCDME), and a dual-stopband FSS (DS-FSS), respectively.

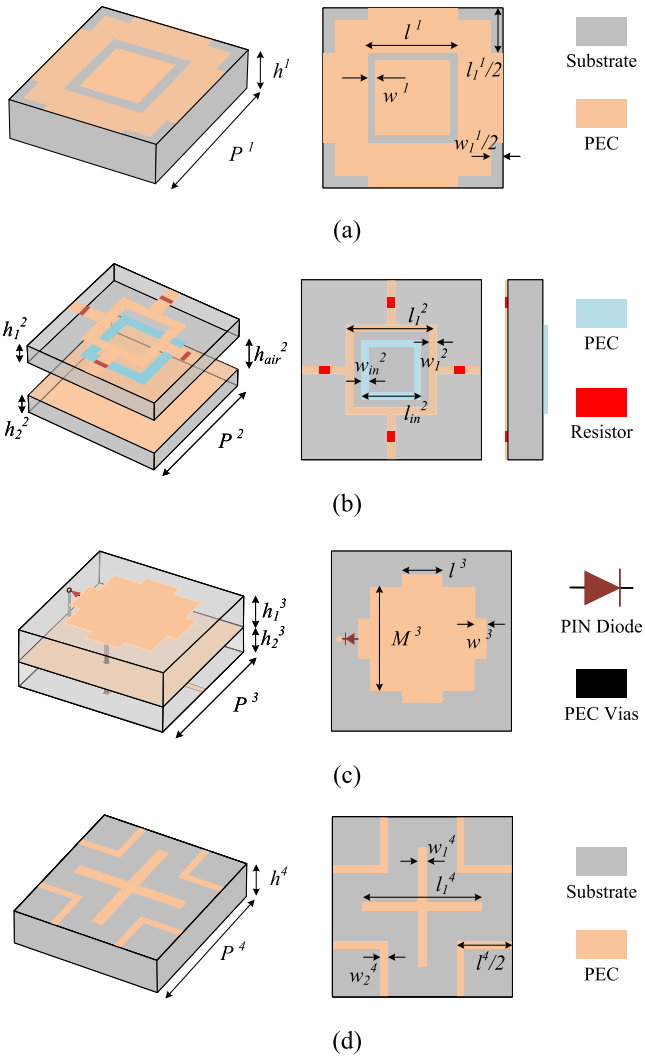

Fig. 6. Structural schematic of (a) DP-FSS, (b) single-/dual-band absorbing metasurface, (c) STCDME, and (d) DS-FSS.

We briefly describe the models for these four structures. Fig. 6(a) shows the DP-FSS model with a square ring slit and a cross slit, where orange represents the PEC and grey is the dielectric substrate. The geometric parameters of model (a)

TABLE I
GEOMETRIC PARAMETERS RANGE OF FOUR STRUCTURES (UNIT: mm)

Param.	Value	Param.	Value	Param.	Value
p^1	20	h^1	[0.5, 0.5, 1.5]	l^1	[13, 1, 18]
w^1	[0.5, 0.5, 1]	l_1^1	[10, 1, 18]	w_1^1	[0.5, 0.5, 1]
p^2	20	h_1^2	[1, 2, 3]	h_2^2	[1, 2, 3]
h_{air}^2	[8, 2, 12]	l_1^2	[8, 1, 13]	w_1^2	[1, 2, 3]
l_2^2	[8, 1, 13]	w_2^2	[1, 2, 3]	p^3	20
h_1^3	[0.5, 0.5, 1.5]	h_2^3	[0.5, 0.5, 1.5]	M^3	[10, 0.5, 13]
w^3	[1, 0.25, 1.5]	l^3	[3, 1, 5]	p^4	20
h^4	[0.5, 0.5, 1.5]	l_1^4	[13, 1, 18]	w_1^4	[0.5, 0.5, 1]
l^4	[10, 1, 18]	w^4	[0.5, 0.5, 1]	$data^1$	500
$data^2$	500	$data^3$	500	$data^4$	500

are p, l, w, l_1, w_1, and h. Fig. 6(b) shows the SDAM model for absorbing EM waves which consists of two substrates, three layers of PEC, and resistors. The blue also represents PEC to make the figure clear, and the red represents the resistor. The SDAM model's geometric parameters are p, h_1, h_2, h_{air}, l_1, w_1, l_2, and w_2. Fig. 6(c) shows the STCDME model which can change the reflection phases by controlling the p-i-n diode state. The red triangle is a p-i-n diode, and the red represents the metal vias. The geometric parameters of model (c) are p, h_1, h_2, M, w, and l. Fig. 6(d) shows the DS-FSS model for reflection EM waves in space. The geometric parameters of model (d) are p, l, w, l_1, w_1, and h. The material constants of the four structures are the same. The dielectric constant of the substrates is 2.2. The dielectric loss tangent of the substrate is 0.0009. The metal is set as 0.02-mm thickness of perfect electric conductor (PEC). In addition, the resistor value of model (b) is 294 Ω. The p-i-n diode of mode (d) equals resistance 5.2 Ω and inductance 30 pH while turned on, and capacitance 40 fF and inductance 30 pH while turned off. Geometric data information is shown in Table I, where "Param." denotes the structure geometric parameter, and "Value" represents the data range and step (start, step, stop). Through CST and Python co-simulation to control geometric parameters, we set a random amount to collect 500 datasets for each structure. The ratio of training, validation, and test datasets is 3:1:1.

These four EM structures have different geometric parameters. We can regard geometric parameters as a vector. Four EM structure geometric vectors' length is 6, 8, 6, and 6, respectively. In addition, the S-parameters' type and frequency range we focus on are not the same; from model (a) to model (d), the frequency we focus on is 1–13 GHz, 5–10 GHz, 1–11 GHz, and 1–13 GHz, respectively. The S-parameters' type we focus on is the transmission amplitude, absorption, reflection phase, and reflection amplitude, respectively. Therefore, we cannot directly use one neural network for these four structure designs. To solve this problem, we use our proposed preprocessing method.

1) We add identification vector t to the structure geometric parameters' vector and S-parameters' vector, where t_1 is the structure type and t_2 is the S-parameters' type.
2) We use the 0-vector method to unify the dimensionality of the structure geometric vector d.
3) We use the interpolation method to unify the dimensionality of the S-parameter vector S with the help of frequency-assisted vector f.
4) We add a random vector r to the structure geometric parameters' vector and S-parameters' vector. The details are shown in Tables II and III.

TABLE II
PREPROCESSING FOR INPUT OF DNN

Vector	t_1	t_2	f	d	r
DP-FSS	0	0	[1, 13]	[p, h, l, w, l_1, w_1, 0, 0]	r_1
SDAM	1	4	[1, 11]	[p, h_1, h_2, h_{air}, l_1, w_1, l_2, w_2]	r_2
STCDME	2	3	[5, 10]	[p, h_1, h_2, M, l, w, 0, 0]	r_3
DS-FSS	3	2	[1, 13]	[p, h, l_1, w_1, l, w, 0, 0]	r_4

TABLE III
PREPROCESSING FOR OUTPUT OF DNN

Vector	t_1	t_2	S	r
DP-FSS	0	0	[S_1, S_2,..., S_{1001},..., S_{1201}]	r_1
SDAM	1	4	[S_1,...,S_{1001}] $\longleftrightarrow$ [S'_1,...,S'_{1201}]	r_2
STCDME	2	3	[S_1,...,S_{501}] $\longleftrightarrow$ [S'_1,...,S'_{1201}]	r_3
DS-FSS	3	2	[S_1, S_2,..., S_{1001},..., S_{1201}]	r_4

Table II shows the input parameters of the FNN. The structure schematics of DP-FSS, SDAM, STCDME, and DS-FSS can be referred to in Fig. 6. The input vectors consist of t_1, t_2, f, d, and r, where t_1 denotes the type of structure, and we have labeled these four different types of structures as 0, 1, 2, and 3, respectively. t_2 is the S-parameters' vector, and we set S_{21} amplitude, S_{21} phase, S_{11} amplitude, S_{11} phase, and absorptive rate as 0, 1, 2, 3, and 4, respectively. The microwave absorptive rate is shown in (12), where Ab is the absorptive rate, S_{11} is the reflection amplitude, S_{21} is the transmission amplitude, and mag means the magnitude value. f is the frequency vector. d is the structure geometric parameter, and we achieve the same dimensionality of the structure geometric dimension parameter for different structures by adding 0-vector. r is the random auxiliary vector used for increasing training data. The final input vector is $X = [t_1, t_2, f, d, r]$.

Table III shows the output parameters of the FNN. Vectors t_1 and t_2 are the same as in Table II, used to confirm the prediction results. Vector S is the S-parameter results. We achieve the same dimensionality for different structural S-parameters by the interpolation method. The final output vector is $Y = [t_1, t_2, S, r]$. Furthermore, we use the amplitude values for the amplitude and take the processing shown in (13) for the phase to control the different structures' differences in the S-parameters

$$Ab = 1 - \text{mag}(S_{11})^2 - \text{mag}(S_{21})^2 \tag{12}$$

$$S'_p = o\big[(S_p + 360)\%360\big]/360 \tag{13}$$

where % denotes obtaining the remainder. $(S_p + 360)\%360$ indicates the remainder obtained by dividing $(S_p + 360)$ by 360. This step changes the angle to [0, 360). o indicates that the results are rounded, which is handled to two decimal places in this article. Dividing the final result by 360 ensures

TABLE IV
RELATIONSHIP OF TRAINING TIME AND MAE WITH THE NUMBER OF FNN LAYERS

	DP-FSS		SDAM		STCDME		DS-FSS		Time
	Train	Test	Train	Test	Train	Test	Train	Test	
1 Layer	0.054	0.054	0.061	0.064	9.25	9.13	0.044	0.045	81s
2 Layers	0.021	0.024	0.025	0.046	4.01	5.39	0.017	0.021	119s
3 Layers	0.016	0.019	0.018	0.041	3.8	5.25	0.016	0.019	180s
4 Layers	0.013	0.018	0.017	0.039	3.37	5.15	0.013	0.017	236s

that the range of phase results is consistent with those for other structural amplitude ranges. Equation (13) implements the phase transformation to the range of [0, 1). This step ensures the neural network is trained more rationally for all EM structures, i.e., it avoids focusing on only one EM structure.

After completing the preparation, we proceed with the design of the deep neural network. The design of DNN parameters is done with three steps.

1) We initially designed the FNN based on professional knowledge. For example, the output of FNN, i.e., S-parameters, are smooth curves, and we do not need to pay attention to individual outliers, so we use MAE as the loss function of FNN. MAE and mean squared error (MSE) are common loss functions calculated as the following equations:

$$\text{MAE} = \frac{1}{n}\sum_{i=1}^{n}\left|Y_i - \hat{Y}_i\right| \tag{14}$$

$$\text{MSE} = \frac{1}{n}\sum_{i=1}^{n}\left(Y_i - \hat{Y}_i\right)^2 \tag{15}$$

where Y_i is the actual value, $\hat{Y}_i$ is the predicted value, and n is the data number. In addition, ReLU can alleviate the disappearance of gradient descent and accelerate the convergence of the network, so we use ReLU for the hidden layer activation function. We have normalized the data, and Sigmoid simplifies the understanding of the model, which is used as the output layer activation function.

2) We design the layer's numbers by comparing the training time of the FNN and the MAE of the predicted results under different numbers of layers. The comparison results are shown in Table IV. As the number of layers increases, the MAE between the predicted and actual results for the four structures becomes progressively more minor. But the MAE change rate is gradually slowing down. At the same time, the time for training DNN increases linearly. Meanwhile, we observe that when the hidden layers are changed from three to four layers, the change in the test data is not significant, although the MAE of the training data still decreases. Therefore, we choose the network architecture with three hidden layers.

3) The final step is to complete each layer's neuron numbers' design through the random search algorithm [37]. In the second step, we fixed the number of each layer's neural neurons as 1000. In the random search algorithm, we initially set a larger space for the initial search. Then, we perform a secondary search and finish the number of neurons' design.

TABLE V
PARAMETERS OF FORWARD DESIGN DNN

No. of layers	First	Second	Third	Final
No. of input	13	800	1200	1500
No. of output	800	1200	1500	1204
Batch normalization	Yes	Yes	Yes	Yes
Activation function	ReLU	ReLU	ReLU	Sigmoid
Optimizer	Adam			
Loss Function	MAE			

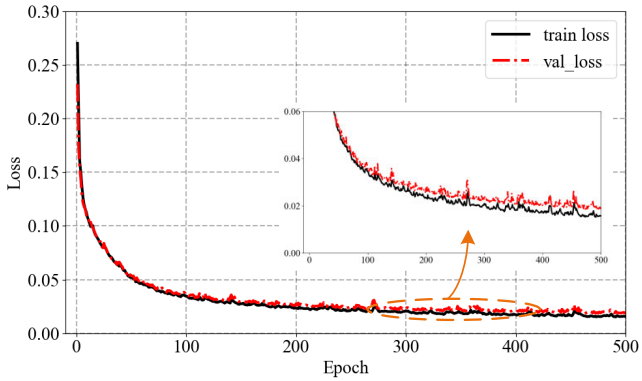

Fig. 7. Loss of the training/validation dataset for FNN.

TABLE VI
DETAIL FOR TRAINING FORWARD DESIGN NEURAL NETWORK

	Data preparation	Train	Test
Time	8h 20m + 12h 30m + 25h + 8h 20m	3m 10s	0.3s
CMS	Intel Xeon Silver 4208	I7-1185G7	

The designed parameters of FNN are shown in Table V. The DNN layers consist of an input layer, three hidden layers, and an output layer. Each layer has 13, 800, 1200, 1500, and 1204 neurons. The training and validation loss function of the training is shown in Fig. 7. Table VI shows the time for collecting data, training/testing the neural network, and computing machine specifications. Data preparation shows four structures' data collecting time, computing machine specification (CMS) Intel Xeon Silver 4208 CPU at 2.10 GHz. Data preparation for different EM structures can be done in parallel. Neural network training and testing is performed by 11th Gen Intel Core i7-1185G7 at 3.00 GHz.

After obtaining the trained neural network, we can use it to predict the structures' S-parameters, as shown in Fig. 8. Fig. 8(a)–(d) shows the transmission amplitude of the DP-FSS, the wave absorption of the SDAM, the reflection phase difference between the two states of the STCDME, and the reflection amplitude of the DS-FSS, respectively. The solid black lines in the figures are the predicted results of the

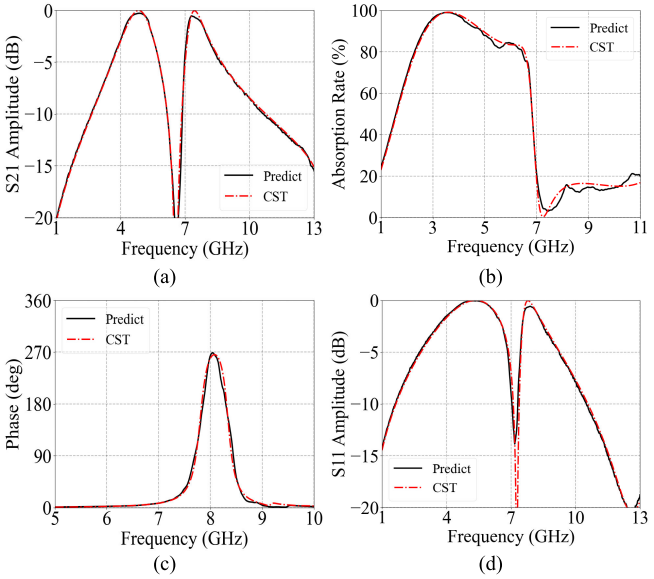

Fig. 8. Results' comparison of forward design network based on the proposed preprocessing method and CST simulation. (a) DP-FSS. (b) SDAM. (c) STCDME. (d) DS-FSS.

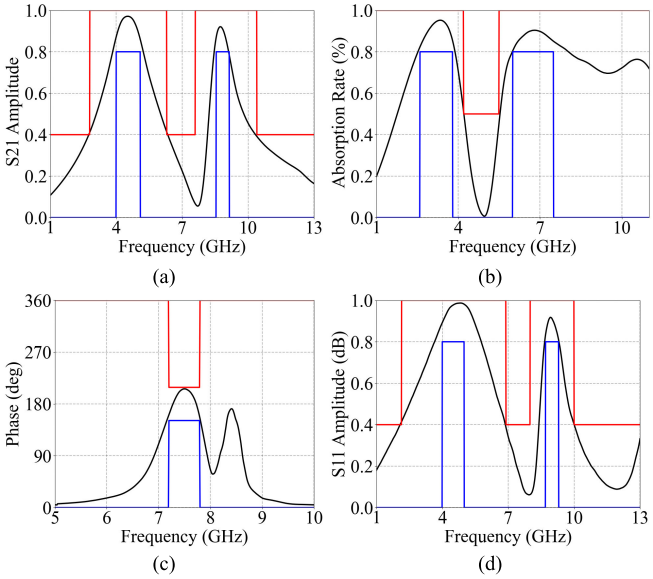

Fig. 9. Fast optimization of S-parameter result curves. (a) DP-FSS. (b) SDAM. (c) STCDME. (d) DS-FSS.

TABLE VII
COMPARISON OF S-PARAMETERS' PREDICTION FOR FOUR DIFFERENT EM STRUCTURES

Structure	S	F		F+I		F+I+R	
	MAE	ACC	MAE	ACC	MAE	ACC	MAE
DP-FSS	0.023	/	0.085	100%	0.023	100%	0.019
SDAM	0.036	/	0.046	100%	0.036	100%	0.035
STCDME	5.07	/	6.02	100%	5.812	100%	5.14
DS-FSS	0.021	/	0.090	100%	0.019	100%	0.018

trained DNN, and the red dashed lines are the CST simulation S-parameters. The predicted neural network results are compared with CST's simulation results and calculated using the MAE loss function. The training/test MAE loss values of the predicted DP-FSS, SDAM, STCDME, and DS-FSS S-parameters' curves versus the actual S-parameters' curves are 0.016/0.019, 0.017/0.036, 3.58/5.14, and 0.015/0.018, respectively.

In Fig. 8, we can see that we accomplish the prediction of different structures with different S-parameters by one neural network. Table VII shows comparison of the FNN prediction results after 500 iterations using several methods. S denotes the single EM structure neural network, F denotes the filling method, I denotes the identification method, and R represents the random auxiliary vector method. MAE represents the difference between the predicted and actual results. ACC denotes the neural network prediction's accuracy of the corresponding S-parameters through the structural parameters, assisted by the identification vector. The comparison shows that the proposed F + I + D method completes the discrimination of the prediction results' correctness and improves the network accuracy.

Based on the fast response and high accuracy property of the designed FNN, we can use it, combining the optimization algorithm, to optimize the EM structure quickly and get the S-parameter response. We optimize by setting the curve range through the following equation [15]:

$$L_S = (S - S_{\min})(S - S_{\max})^{\mathrm{T}} + \left|(S - S_{\min})(S - S_{\max})^{\mathrm{T}}\right| \quad (16)$$

where $S_{\min}/S_{\max}$ is the lower/higher limit of the S-parameters, T is the transposition, and L_S is the optimization objective, whose value gets smaller means better optimization. The optimization results are shown in Fig. 9, which presents good performance for optimizing multiple EM structures.

Part of the designed EM structures are fabricated and measured to validate the proposed design methodology, as shown in Fig. 10(a)–(f). We fabricate elements of 20 × 20 DP-FSS and DS-FSS, respectively. Schematics of the fabricated DP-FSS and DS-FSS are shown in Fig. 10(a) and (b). Fig. 10(c)–(f) shows the measurement environment and schematic of DP-FSS/DS-FSS. We put the fabrications in the middle of the absorbing material and used one horn as the emitting source and the other as the receiving source. We placed two horns on both sides of the DP-FSS to measure its transmission coefficient. For the DS-FSS, we put two horns on one side to measure the reflection coefficient.

The final measurement results are obtained through the different horn crossover band tests in an anechoic chamber, as shown in Fig. 11. The slight deviations between the experiment and simulation are attributed to calculation, fabrication, measurement errors, etc. But in general, the measurement results are in good agreement with the simulation results, which verifies the reliability of the design methodology.

B. Example 2: Multiple EM Structures Inverse Designs

In this section, we use the proposed preprocessing method to complete the inverse design of different EM structures. We still use DP-FSS, SDAM, STCDME, and DS-FSS, shown in Fig. 6 as examples. The data collected for each structure are 500. In forward design, we get the structures' S-parameters

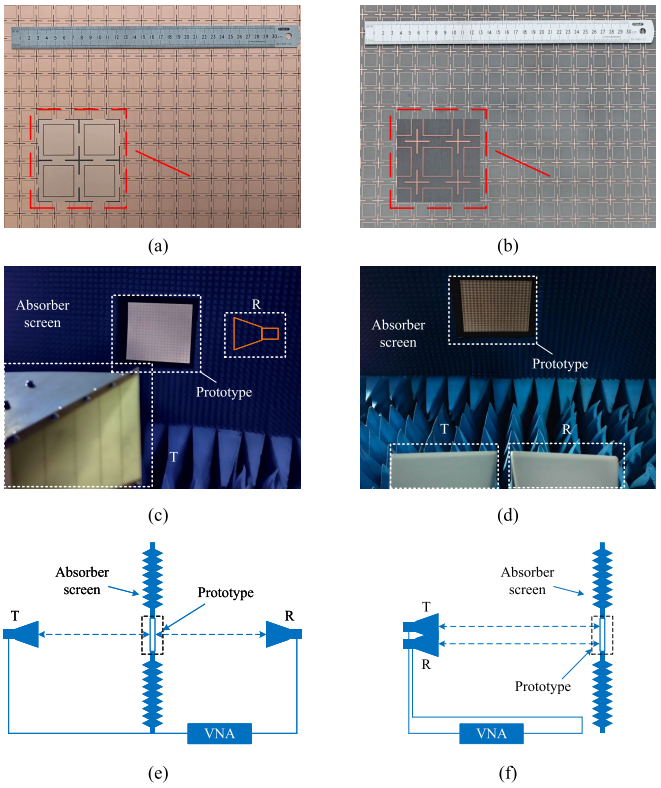

Fig. 10. Fabricated schematic of (a) DP-FSS and (b) DS-FSS. Measurement environment of (c) DP-FSS and (d) DS-FSS. Measurement schematic of (e) DP-FSS and (f) DS-FSS.

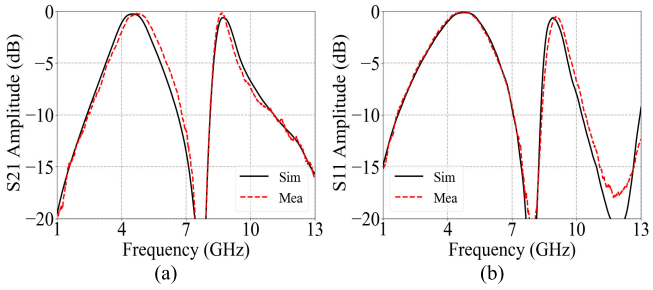

Fig. 11. Measurement and simulation results' comparison of (a) DP-FSS (b) DS-FSS.

by feeding the structures' geometric parameters into the DNN. Unlike the forward design, we get the structure geometric parameters in the inverse design by feeding the DNN with S-parameters. In the previous subsection of the forward design process, we combined the identification vector t, frequency vector f, structure geometric parameters vector d, and the random auxiliary vector r into the input vector X, i.e., $X = [t_1, t_2, f, d, r]$. The identification vector t, S-parameters' vector S, and random auxiliary vector r are into an output vector Y, i.e., $Y = [t_1, t_2, S, r]$. In this section for the inverse design, we only need to change some vectors' positions in FNN. That is, we change the position of the structure geometric parameters' vector d and S-parameters' vector S in FNN and get the new input $X = [t_1, t_2, f, S, r]$ and output $Y = [t_1, t_2, d, r]$ for INN.

The inverse design is a mapping from high dimensionality to low dimensionality. The design optimization process of INN

TABLE VIII
PARAMETERS OF INVERSE DESIGN DNN

No. of layers	First	Second	Third	Final
No. of input	1206	800	500	300
No. of output	800	500	300	11
Batch normalization	Yes	Yes	Yes	Yes
Activation function	ReLU	ReLU	ReLU	Sigmoid
Optimizer	Adam			
Loss Function	MSE			

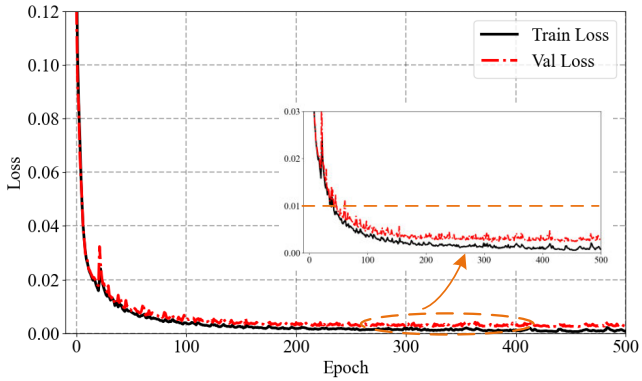

Fig. 12. Loss of the training/validation dataset for INN.

is the same as that of FNN and is not elaborated here. The final designed neural network parameters are shown in Table VIII. We still use Adam as the optimizer. Unlike the FNN design, the output of INN, i.e., structural parameters, is not continuous data, and we use MSE as the loss function.

The training and validation dataset loss of INN is shown in Fig. 12, which shows a good training performance. The training/testing time for inverse design neural network is 1 m 40 and 0.2 s, respectively. We compared different preprocessing methods' S-parameters prediction results after 500 iterations, and the comparison results are shown in Table IX. It can be found that the proposed method enables the prediction of multiple EM structures' geometric parameters in one neural network, with guaranteed prediction accuracy and improved accuracy. Notably, part of the structure sizes predicted by single INN are less accurate than those predicted by multiple INN. For example, DP-FSS, STCDME, and DS-FSS have MAE values of 0.139, 0.305, and 0.105 when trained by separate networks, but the MAE values concluded by F + I + R INN are 0.116, 0.146, and 0.07. This may be because more structures correspond to more data, allowing the neural network to learn more about the S-parameters. This aspect certainly deserves further research.

Fig. 13 shows four EM structure prediction results by the INN. The left figures show the S-parameters, where the black solid lines are the target curves, i.e., the input of the INN. The output of the INN is the structure geometric parameters, i.e., the white rectangle on the right of Fig. 13, and it is compared with the actual structural parameters of the target curve, i.e., the red rectangle. Based on the predicted structural dimensions

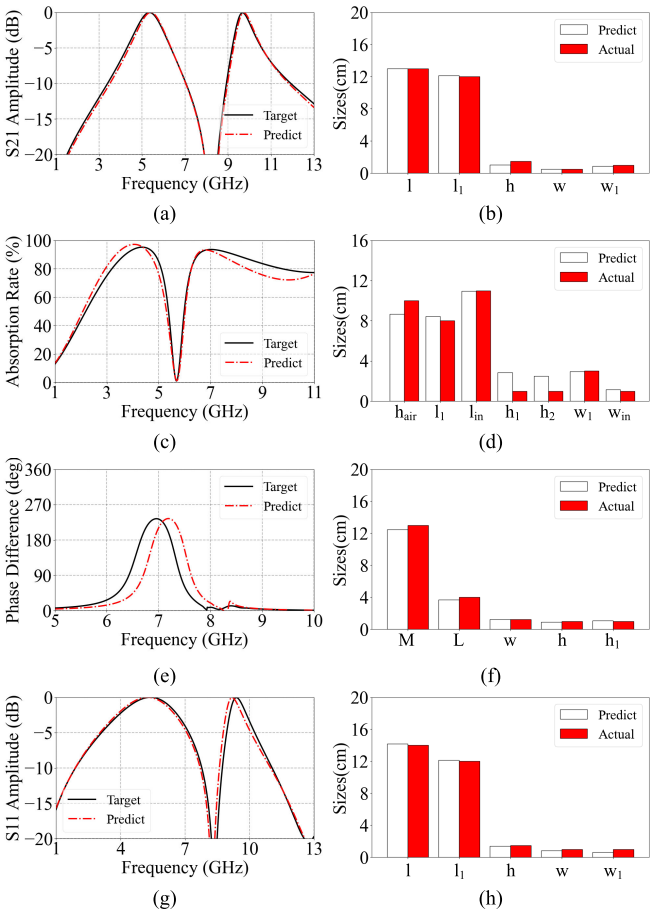

Fig. 13. Different EM structures' inverse design results with only one network based on the proposed preprocessing method. (a) DP-FSS transmission coefficient. (b) DP-FSS structure size. (c) SDAM state phase difference. (d) SDAM structure size. (e) STCDME absorption rate. (f) STCDME structure size. (g) DS-FSS reflection coefficient. (h) DS-FSS structure size.

TABLE IX
COMPARISON OF PREDICTION GEOMETRIC PARAMETERS RESULTS FOR FOUR STRUCTURES

Structure	S	F		F+I		F+I+R	
	MAE	ACC	MAE	ACC	MAE	ACC	MAE
DP-FSS	0.139	/	0.127	100%	0.127	100%	0.116
SDAM	0.503	/	0.767	100%	0.625	100%	0.602
STCDME	0.305	/	0.150	100%	0.153	100%	0.146
DS-FSS	0.105	/	0.082	100%	0.091	100%	0.070

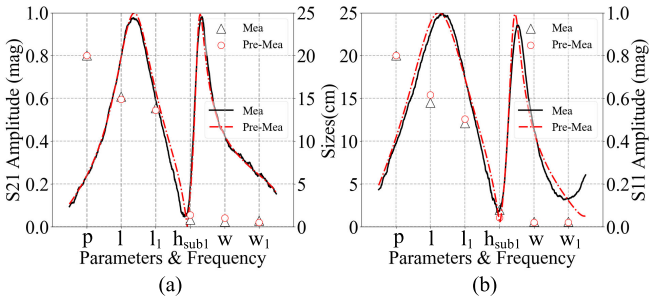

Fig. 14. Predicting measurement results by the INN. (a) DP-FSS. (b) DS-FSS.

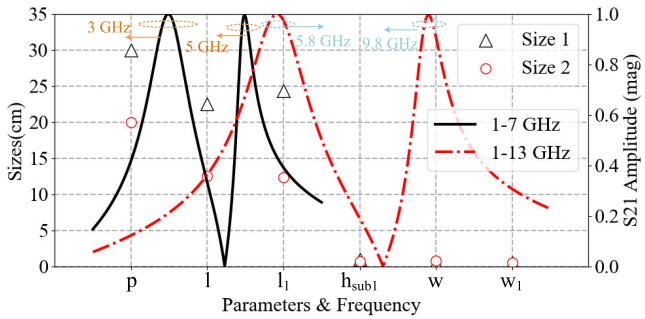

Fig. 15. Doubling frequency design of DP-FSS based on INN.

and identification vector values, we can quickly simulate and obtain S-parameters by joint modeling with CST and Python software. The obtained S-parameters are shown as the red dashed lines in the left panel of Fig. 13. It can be seen that the predicted structures' S-parameters have a good fit with the target curves. The predicted structures' S-parameters of the STCDME and SDAM structures differ slightly from the target curves due to their complex structures and limited data. The S-parameters are sensitive to changes in structural parameters, so more accurate structure geometric parameters are necessary. In this work, we select the same training data numbers for each structure. The targeted selection of training data numbers for each structure can selectively improve the prediction results. Overall, Fig. 13 predicted results fit the target curves well. It provides a good referring structure model with little error.

In addition, the inverse design provides us with new design ideas as given below.

1) Generating structural models based on measurement data. We can use the inverse model to predict the structure model and sizes based on measurement results and generate a similar structural model for reference. As shown in Fig. 14, the black curves are the measurement results, and the corresponding black triangles are the prototype sizes. We use the measurement results as the INN input, which obtain structural dimensions shown as the red circles, and the red dashed lines correspond to S-parameters of predicted sizes. Of course, the predicted results are not guaranteed to agree with the actual structural dimensions due to the multivalue problem of inverse design, which may be more like providing a reference design model.
2) Completing the design quickly when the frequency is changed or multiplied. We take structure one DP-FSS as an example to realize the fast design of doubling frequency. The results are shown in Fig. 15. The black curve shows the designed 1–7-GHz DP-FSS, and the black triangle "Size 1" is its structure size. We use the black curve as the input of INN, combined with the filling method used in this article, to complete the prediction of the structure, and the predicted structure size is shown as the red circle "Size 2." The red curve is obtained based on predicted "Size 2." It can be seen the INN quickly assists in accomplishing the doubling frequency design of the DP-FSS with good performance.

C. Discussion

This article focuses on the idea of using one neural network for the design and optimization of different structures. To implement this idea, we initially proposed and used two filling methods to unify the vector lengths. In addition, we propose the identification method, which is equivalent to integrating the classification problem of EM structures into the regression problem, improving the reliability of the neural network. This article contributes to a systematic DL-assisted EM architecture design, simplifying the framework of the system. Of course, some work still deserves to be further developed, such as better filling methods, for example, how to better plan the prediction of multiple structures by one neural network.

V. Conclusion

This article presents a method for using a single neural network to optimize multiple EM structure designs through proposed preprocessing techniques, which substantially simplifies the AI-assisted EM design framework for multiple structures. In contrast to prior AI-based EM design methods, i.e., one neural network for one structure, our approach maximizes the usage of neural networks while reducing design complexity. The main results of this work are as follows.

1) We propose two filling methods to normalize vector length, i.e., 0-vector and linear interpolation filling methods, the identification method to validate the prediction type accuracy and the random auxiliary vector method to increase the accuracy. The proposed method achieves AI-based multiple EM structures' design, fully using the neural network and simplifying the design framework for multi-EM structures.
2) We apply our method in the FNN and design DP-FSS, DAM, STCDME, and DS-FSS structures. The MAE loss values of the FNN predicted and actual results are 0.019, 0.035, 5.14, and 0.018. We fabricate DP-FSS and DS-FSS, which are measured in an anechoic chamber. The measurement results are in good agreement with the simulated results, proving the proposed method's reliability.
3) We apply our method in the INN with four structures. The MAE loss values of the INN predicted and actual results are 0.116, 0.602, 0.146, and 0.07. We also investigate the acquisition of INN input data and the way to improve the prediction results' reliability.

While we use only four EM metasurface structures as examples in this article, these techniques can also be applied to other EM structure designs, such as antennas and microwave circuits. Our proposed method significantly reduces the complexity of AI-based multiple EM structure designs, thereby paving the way for a more efficient and less time-consuming AI-based process in the realm of EM structure designs.

References

[1] B. A. Munk, *Frequency Selective Surfaces: Theory and Design*. Hoboken, NJ, USA: Wiley, 2005.

[2] J. C. Liang et al., "An angle-insensitive 3-bit reconfigurable intelligent surface," *IEEE Trans. Antennas Propag.*, vol. 70, no. 10, pp. 8798–8808, Oct. 2022.

[3] T. Hong, M. Wang, K. Peng, Q. Zhao, and S. Gong, "Compact ultra-wide band frequency selective surface with high selectivity," *IEEE Trans. Antennas Propag.*, vol. 68, no. 7, pp. 5724–5729, Jul. 2020.

[4] Q. Guo, Z. Li, J. Su, L. Y. Yang, and J. Song, "Dual-polarization absorptive/transmissive frequency selective surface based on tripole elements," *IEEE Antennas Wireless Propag. Lett.*, vol. 18, no. 5, pp. 961–965, May 2019.

[5] H. Xu et al., "Switchable complementary diamond-ring-shaped metasurface for radome application," *IEEE Antennas Wireless Propag. Lett.*, vol. 17, pp. 2494–2497, 2018.

[6] A. Chatterjee and S. K. Parui, "Performance enhancement of a dual-band monopole antenna by using a frequency-selective surface-based corner reflector," *IEEE Trans. Antennas Propag.*, vol. 64, no. 6, pp. 2165–2171, Jun. 2016.

[7] Y. Liu et al., "Reconfigurable intelligent surfaces: Principles and opportunities," *IEEE Commun. Surveys Tuts.*, vol. 23, no. 3, pp. 1546–1577, 3rd Quart., 2021.

[8] P. Ni, M. Li, R. Liu, and Q. Liu, "Partially distributed beamforming design for RIS-aided cell-free networks," *IEEE Trans. Veh. Tech.*, vol. 71, no. 12, pp. 13377–13381, Dec. 2022.

[9] Y. Liu, K. Li, Y. Jia, Y. Hao, S. Gong, and Y. J. Guo, "Wideband RCS reduction of a slot array antenna using polarization conversion metasurfaces," *IEEE Trans. Antennas Propag.*, vol. 64, no. 1, pp. 326–331, Jan. 2016.

[10] Y. Shang, Z. Shen, and S. Xiao, "Frequency-selective rasorber based on square-loop and cross-dipole arrays," *IEEE Trans. Antennas Propag.*, vol. 62, no. 11, pp. 5581–5589, Nov. 2014.

[11] L. Zhang et al., "Space-time-coding digital metasurfaces," *Nature Commun.*, vol. 9, no. 1, p. 4334, Oct. 2018.

[12] N. Hu et al., "Design of ultrawideband energy-selective surface for high-power microwave protection," *IEEE Antennas Wireless Propag. Lett.*, vol. 18, no. 4, pp. 669–673, Apr. 2019.

[13] J. Wang et al., "Deep neural network with data cropping algorithm for absorptive frequency-selective transmission metasurface," *Adv. Opt. Mater.*, vol. 10, no. 13, Jul. 2022, Art. no. 2200178.

[14] P. Naseri and S. V. Hum, "A generative machine learning-based approach for inverse design of multilayer metasurfaces," *IEEE Trans. Antennas Propag.*, vol. 69, no. 9, pp. 5725–5739, Sep. 2021.

[15] Z. Wei et al., "Equivalent circuit theory-assisted deep learning for accelerated generative design of metasurfaces," *IEEE Trans. Antennas Propag.*, vol. 70, no. 7, pp. 5120–5129, Jul. 2022.

[16] Z. Wei et al., "Automated antenna design via domain knowledge-informed reinforcement learning and imitation learning," *IEEE Trans. Antennas Propag.*, vol. 71, no. 7, pp. 5549–5557, Jul. 2023.

[17] D. R. Prado, J. A. López-Fernández, M. Arrebola, and G. Goussetis, "Support vector regression to accelerate design and crosspolar optimization of shaped-beam reflectarray antennas for space applications," *IEEE Trans. Antennas Propag.*, vol. 67, no. 3, pp. 1659–1668, Mar. 2019.

[18] D. R. Prado, J. A. López-Fernández, M. Arrebola, M. Rodriguez-Pino, and G. Goussetis, "Wideband shaped-beam reflectarray design using support vector regression analysis," *IEEE Antennas Wireless Propag. Lett.*, vol. 18, no. 11, pp. 2287–2291, Nov. 2019.

[19] J. A. Hodge, K. V. Mishra, and A. I. Zaghloul, "RF metasurface array design using deep convolutional generative adversarial networks," in *Proc. IEEE Int. Symp. Phased Array Syst. Technol. (PAST)*, Oct. 2019, pp. 1–6.

[20] J. A. Fan, "Generating high performance, topologically-complex metasurfaces with neural networks," in *Proc. Conf. Lasers Electro-Optics (CLEO)*, May 2019, pp. 1–2.

[21] M. Abdullah and S. Koziel, "Supervised-Learning-Based development of multibit RCS-reduced coding metasurfaces," *IEEE Trans. Microwave Theory Techn.*, vol. 70, no. 1, pp. 264–274, Jan. 2022.

[22] S. Koziel and M. Abdullah, "Machine-learning-powered EM-based framework for efficient and reliable design of low scattering metasurfaces," *IEEE Trans. Microwave Theory Techn.*, vol. 69, no. 4, pp. 2028–2041, Apr. 2021.

[23] Z. Ž. Stankovic, D. I. Olcan, N. S. Doncov, and B. M. Kolundžija, "Consensus deep neural networks for antenna design and optimization," *IEEE Trans. Antennas Propag.*, vol. 70, no. 7, pp. 5015–5023, Jul. 2022, doi: 10.1109/TAP.2021.3138220.

[24] J. Zhang, J. Xu, Q. Chen, and H. Li, "Machine-learning-assisted antenna optimization with data augmentation," *IEEE Antennas Wireless Propag. Lett.*, vol. 22, no. 8, pp. 1932–1936, Aug. 2023.

[25] E. Zhu, Z. Wei, X. Xu, and W.-Y. Yin, "Fourier subspace-based deep learning method for inverse design of frequency selective surface," *IEEE Trans. Antennas Propag.*, vol. 70, no. 7, pp. 5130–5143, Jul. 2022.
[26] R. Cong, N. Liu, X. Li, H. Wang, and X. Sheng, "Design of wideband frequency selective surface based on the combination of the equivalent circuit model and deep learning," *IEEE Antennas Wireless Propag. Lett.*, vol. 22, no. 9, pp. 2110–2114, Sep. 2023.
[27] P. Wang et al., "A machine learning framework for the design of STCDME structures in RIS applications," *IEEE Trans. Microwave Theory Techn.*, vol. 72, no. 3, pp. 1467–1479, Mar. 2024.
[28] F. Wen, J. Jiang, and J. A. Fan, "Progressive-growing of generative adversarial networks for metasurface optimization," 2019, *arXiv:1911.13029*.
[29] H. P. Wang et al., "Deep learning designs of anisotropic metasurfaces in ultrawideband based on generative adversarial networks," *Adv. Intell. Syst.*, vol. 2, no. 9, Sep. 2020, Art. no. 2000068.
[30] S. An et al., "Multifunctional metasurface design with a generative adversarial network," *Adv. Opt. Mater.*, vol. 9, no. 5, Mar. 2021, Art. no. 2001433.
[31] Z. Wei et al., "Fully automated design method based on reinforcement learning and surrogate modeling for antenna array decoupling," *IEEE Trans. Antennas Propag.*, vol. 71, no. 1, pp. 660–671, Jan. 2023, doi: 10.1109/TAP.2022.3221613.
[32] P. Naseri, S. Pearson, Z. Wang, and S. V. Hum, "A combined machine-learning/optimization-based approach for inverse design of nonuniform bianisotropic metasurfaces," *IEEE Trans. Antennas Propag.*, vol. 70, no. 7, pp. 5105–5119, Jul. 2022.
[33] D. Shi, C. Lian, K. Cui, Y. Chen, and X. Liu, "An intelligent antenna synthesis method based on machine learning," *IEEE Trans. Antennas Propag.*, vol. 70, no. 7, pp. 4965–4976, Jul. 2022.
[34] Z. Zhou, Z. Wei, J. Ren, Y. Yin, G. F. Pedersen, and M. Shen, "Representation learning-driven fully automated framework for the inverse design of frequency-selective surfaces," *IEEE Trans. Microw. Theory Techn.*, vol. 71, no. 6, pp. 2409–2421, Jun. 2023.
[35] L. N. Kanal, "Perceptron," in *Encyclopedia Computer Science*. Chichester, U.K.: Wiley, 2003, pp. 1383–1385. [Online]. Available: https://dl.acm.org/doi/abs/10.5555/1074100.1074686
[36] Z. Zhou et al., "A high-quality data acquisition method for machine-learning-based design and analysis of electromagnetic structures," *IEEE Trans. Microw. Theory Techn.*, vol. 71, no. 10, pp. 4295–4306, Oct. 2023.
[37] J. Bergstra and Y. Bengio, "Random search for hyper-parameter optimization," *J. Mach. Learn. Res.*, vol. 13, no. 2, pp. 1–25, Feb. 2012.

Peng Wang (Graduate Student Member, IEEE) was born in Anqing, Anhui, China. He received the B.Sc. and M.Eng. degrees in electronic engineering from Xidian University, Xi'an, China, in 2017 and 2020, respectively. He is currently pursuing the Ph.D. degree with the Antennas, Propagation, and Millimeterwave Systems (APMS) Section, Department of Electronic Systems, Aalborg University, Aalborg, Denmark.

His current research interests include high-performance metasurface design and machine-learning-based methods for the design and analysis of metasurface.

Zhenning Li was born in China in 1994. He received the B.Sc. and M.Eng. degrees in electronic engineering from Xidian University, Xi'an, China, in 2017 and 2020, respectively.

He is currently a Research Associate with the Aerospace Information Research Institute, Chinese Academy of Sciences, Beijing, China. His current research interests include electromagnetic metamaterials, antenna theory and engineering, and RF circuit systems.

Chao Luo was born in Shandong, China. He received the B.Sc. degree from Northeast Forestry University, Harbin, China, in 2012, and the M.Eng. degree from the University of Electronic Science and Technology of China, Chengdu, China, in 2015.

He is currently a Research Associate with the Aerospace Information Research Institute, Chinese Academy of Sciences, Beijing, China. His current research interests include miniaturized multichannel components and electromagnetic measurement.

Zhaohui Wei (Graduate Student Member, IEEE) was born in Shandong, China. He received the B.Sc. and M.Eng. degrees in electronic engineering from Xidian University, Xi'an, China, in 2017 and 2020, respectively. He is currently pursuing the Ph.D. degree with the Antennas, Propagation and Millimeter-Wave Systems Section, Department of Electronic Systems, Aalborg University, Aalborg, Denmark.

His research interests include filtering antenna, frequency-selective surface, and deep-learning-based methods for the design and analysis of antenna systems.

Tong Wu was born in China in 2003. He is currently pursuing the B.Eng. degree with the College of Information Science and Electronic Engineering, Zhejiang University, Hangzhou, China.

He also communicates with the Antennas, Propagation, and Millimeterwave Systems Section for personal distance learning. His current research interests include small frequency-selective surface design and deep-learning-based methods for the design and analysis of frequency-selective surface.

Wen Jiang (Senior Member, IEEE) was born in Shandong, China, in 1985. He received the B.S. and Ph.D. degrees from Xidian University, Xi'an, China, in 2008 and 2012, respectively.

He is currently the Vice-Director of the National Key Laboratory of Science and Technology on Antennas and Microwaves, Xidian University, where he is also a Full Professor. His current research interests include electromagnetic scattering theory and technology, antenna theory and engineering, and electromagnetic measurement theory technology.

Tao Hong (Senior Member, IEEE) was born in Shaanxi, China, in December 1983. He received the B.S. and Ph.D. degrees from Xidian University, Xi'an, China, in 2006 and 2011, respectively.

He is currently a Full Professor with Xidian University. His current research interests include electromagnetic scattering theory, antenna theory and engineering, and electromagnetic measurement.

Naser Ojaroudi Parchin (Senior Member, IEEE) received the Ph.D. degree in electrical engineering from the University of Bradford, Bradford, U.K., in 2020.

He was a Postdoctoral Research Assistant with the Faculty of Engineering and Informatics, University of Bradford. He was a Research Fellow in the SATNNEX V Project, funded by the European Space Agency. From 2014 to 2018, he was with the APMS Section, Aalborg University, Aalborg, Denmark. In 2016, he was a Visiting Researcher with Ankara University, Ankara, Turkey. From 2018 to 2020, he was a Marie Curie Research Fellow in the H2020-ITN-SECRET Project, funded by EU Commission, targeting 5G mobile small cells. He is currently an Assistant Professor (a Lecturer) with Edinburgh Napier University, Edinburgh, U.K. He has over 12 years of research experience in antennas and microwave engineering. His articles have more than 7400 citations with 49 H-index, reported by Google Scholar. His score is higher than 95% of all RG members' scores. He is the author and coauthor of several books/book chapters and more than 300 technical journals and conference papers. His research interests include phased arrays, MIMO systems, smartphone antennas, SAR/user-impact, full-duplex diversity, 5G antennas, implementable and biomedical sensors, RFID tag antennas, millimeter-wave and terahertz components, fractal structures, metamaterials/metasurfaces, PCB realization, Fabry resonators, EBG/FSS-inspired radiators, microwave filters, reconfigurable structures, and wireless propagation.

Dr. Parchin is a member of the Marie Curie Alumni Association (MCAA) and the European Association on Antennas and Propagation (EurAAP). He was a recipient and a co-recipient of various Awards and Grants for research publications, such as the 2018 Research Development Fund, 2020/2021 MDPI Travel Award, the Best Paper Awards at URSI Symposium 2019, the 5G Summit 2019, U.K. URSI Festival 2020, IMDC 2021, and ITC-Egypt 2022. He is a Research Grant Reviewer of the Dutch Science Council (NWO). He is also an active reviewer in various high-ranking journals and publishers, such as IEEE TRANSACTIONS, IEEE ACCESS/LETTERS, IET, Wiley, Springer, Elsevier, and MDPI. He is appointed as a guest editor and topic board of several MDPI journals. He was included in the World's Top Scientists list, in 2016 and 2020–2023.

Gert Frølund Pedersen (Senior Member, IEEE) was born in 1965. He received the B.Sc.E.E. degree (Hons.) in electrical engineering from the College of Technology, Dublin Institute of Technology, Dublin, Ireland, in 1991, and the M.Sc.E.E. and Ph.D. degrees from Aalborg University, Aalborg, Denmark, in 1993 and 2003, respectively.

Since 1993, he has been with Aalborg University, as a Full Professor heading the Antennas, Propagation, and Millimeter-Wave Systems Section with 25 researchers. He is also the Head of the Doctoral School on Wireless Communication with 40 Ph.D. students enrolled. He has published more than 500 peer-reviewed articles, six books, and 12 book chapters, and holds more than 50 patents. His research interests include radio communication for mobile terminals, especially small antennas, diversity systems, propagation, and biological effects.

Ming Shen (Senior Member, IEEE) was born in Yuxi, China. He received the M.Sc. degree in electrical engineering from the University of Chinese Academy of Sciences (UCAS), Beijing, China, in 2005, and the Ph.D. degree in wireless communications from Aalborg University, Aalborg, Denmark, in 2010, with the Spar Nord Annual Best Thesis Nomination.

He is currently an Associate Professor in RF and mm-wave circuits and systems with the Department of Electronic Systems, Aalborg University. He has 20 years of experience in RF and millimeter-wave circuits and systems, including 12 years of experience in CMOS RF/mixed-signal IC design. He is also the Grant Holder and PI of two Danish national research projects and the Management Committee Member Substitute from Denmark in the EU COST Action IC1301 with the aim to gather international efforts and address efficient wireless power transmission technologies. His current research interests include circuits and antennas for 5G and satellite communications, low-power CMOS RF and millimeter-wave circuits and systems, circuits and systems for biomedical imaging, and artificial intelligence.

Dr. Shen is a TPC Member of IEEE Nordic Circuits and Systems Conference (NORCAS). He also serves as a reviewer for IEEE and Kluwer.